

Functionalized Pd/ZnO Nanowires for Nanosensors

Oleg Lupan,* Vasile Postica, Rainer Adelung,* Frédéric Labat, Ilaria Ciofini, Ulrich Schürmann, Lorenz Kienle, Lee Chow, Bruno Viana, and Thierry Pauporté

A method for surface doping and functionalization of ZnO nanowires (NWs) with Pd (Pd/ZnO) in a one-step process is presented. The main advantage of this method is to combine the simultaneous growth, surface doping, and functionalization of NWs by using electrochemical deposition (ECD) at relatively low temperatures (90 °C). Our approach essentially reduces the number of technological steps of nanomaterial synthesis and final nanodevices fabrication with enhanced performances. A series of nanosensor devices is fabricated based on single Pd/ZnO NWs with a radius of about 80 nm using a FIB/SEM system. The influence of Pd nominal composition in Pd/ZnO NW on the H₂ sensing response is studied in detail and a corresponding mechanism is proposed. The results demonstrate an ultra-high response and selectivity of the synthesized nanosensors to hydrogen gas at room temperature. The optimal concentration of PdCl₂ in the electrolyte to achieve extremely sensitive nanodevices with a gas response (S_{H_2}) $\approx 1.3 \times 10^4$ (at 100 ppm H₂ concentration) and relatively high rapidity is 0.75 μ M. Theoretical calculations on Pd/ZnO bulk and functionalized surface further validated the experimental hypothesis. Our results demonstrate the importance of noble metal presence on the surface due to doping and functionalization of nanostructures in the fabrication of highly-sensitive and selective gas nanosensors operating at room temperature with reduced power consumption.

Nanoscale sized clusters of noble metals such as Pd, Pt, Au, Ag, Rh, and Ru, are known to act as effective catalysts^[1,2] and play a vital role in the improvement of the semiconducting oxides sensing properties and photocatalytic activities.^[3–5] A number of methods

has been proposed to incorporate these metals into semiconducting oxides micro- and nanostructures in order to improve their UV- and gas-sensing properties in the most efficient way. The most well-documented methods are adsorption, doping,^[6,7] surface functionalization (decorating, hybridization, loading, impregnating),^[3,8] and composing.^[9] Among all noble metals, Pd-doping/incorporation has been demonstrated to show the highest efficiency in the detection of H₂ gas.^[2,5,10] Such radically improved performances can be attributed to both chemical and electronic sensitizations.^[5] The presence of Pd nanoparticles on ZnO greatly improves the room temperature catalytic activity due to the high H₂ solubility in Pd which gives higher concentration of clusters (catalytic centers) and lowers the saturation rate of response and recovery processes.^[11]

The detection mechanism of sensors based on NWs in most cases is based on the modulation of the conduction channel/electron depleted region (EDR).^[3,6] In the case of surface functionalization, the

Schottky barriers are formed at the Pd/semiconducting oxide interface due to higher work function of Pd compared to ZnO,^[3,12] leading to more narrowed conduction channel (extension of EDR). After exposure to H₂ gas, the formation of PdH_x phases with lower work function can take place,^[2,12] which lower the height of the Schottky barrier and expand the conduction channel width (suppression of EDR).^[6,12] This type of mechanism is related to electronic sensitization.^[5] Another important sensing mechanism is related to chemical sensitization and is based on dissociation of H₂ molecules into H atoms,^[2,13] which interact with adsorbed oxygen species onto the surface of semiconducting oxide nanostructures. It is not well understood yet which mechanism is more dominant under different operating conditions.^[3,14] However, in the case of surface functionalization with noble metal nanoparticles (NPs) due to the dependence of gas response on size and homogeneity of NPs, density, and space distribution, some issues still need to be resolved in order to improve long term stability and repeatability of sensors.^[3,14] Thus, different methods for efficient control of the NPs deposition are still investigated.^[14]


In this study we demonstrate the outstanding increase in hydrogen gas sensing properties of a single Pd/ZnO NW based nanosensor after surface doping and functionalized with Pd NPs. Both surface doping and functionalization are performed

Dr. O. Lupan, Prof. R. Adelung, Dr. U. Schürmann, Prof. L. Kienle
Institute for Materials Science
Christian Albrechts University Kiel
Kaiserstr. 2, D-24143 Kiel, Germany
E-mail: ollu@tf.uni-kiel.de; ra@tf.uni-kiel.de

Dr. O. Lupan, V. Postica
Department of Microelectronics and Biomedical Engineering
Technical University of Moldova
168 Stefan cel Mare Av., MD-2004 Chisinau, Republic of Moldova

Dr. O. Lupan, Dr. F. Labat, Dr. I. Ciofini, Dr. B. Viana, Dr. T. Pauporté
PSL Research University, Chimie ParisTech-CNRS
Institut de Recherche de Chimie Paris, UMR8247
11 rue P. et M. Curie, 75005 Paris, France

Prof. L. Chow
Department of Physics, University of Central Florida
Orlando, FL 32816-2385, USA

 The ORCID identification number(s) for the author(s) of this article can be found under <https://doi.org/10.1002/pssr.201700321>.

DOI: 10.1002/pssr.201700321

during the NWs growth, which is the main advantage of this proposed method. This effectively reduces the fabrication steps of the final device and excludes many multistep technologies of semiconducting oxides manufacturing. Pd-doped ZnO bulk and functionalized surfaces were also modeled using DFT to obtain insights into the experimental findings. Devices were fabricated via focused ion beam (FIB)/SEM system and showed the ultrasensitive and highly selective response at room temperature with the lowest detection limit (LDL) in the range of sub-ppm (0.015 ppm or 15 ppb). The effect of Pd content was studied in detail, and the respective sensing mechanism was proposed based on theoretical and experimental data. Presented results are of high scientific interest, especially in the field of nanodevice fabrication and for highly sensitive nanosensors.^[2,3,15,16] In this study the influence of junctions between ZnO NWs on gas response (important in the case of networks) is excluded and only the influence of functionalization is investigated. The novelty of this work also lies in getting further insights into the gas sensing mechanism of individual hybrid Pd/ZnO NWs, which is very important from a fundamental point of view.

Experimental Section: The ZnO NWs were grown using electrochemical deposition in a three-electrode electrochemical cell at 90 °C as was reported in previous works.^[6,17,18,19] Synthesis, surface doping, and functionalization with Pd NPs of ZnO NWs were achieved in one step-process by adding PdCl₂ solution (Alfa Aesar) in the electrolyte solution with a concentration range of 0.25–1.50 μM. F-doped SnO₂ (FTO) polycrystalline films (sheet resistance 10 Ω sq) were used as substrates and as working electrode (WE) for the electrodeposition of Pd/ZnO NW arrays.^[17,18] The procedure of substrates cleaning was reported in previous works.^[17,18] During the deposition process, the angular speed of WE was set at $\omega = 300 \text{ rotation min}^{-1}$ (rpm). Total deposition time was 7000–9000 s.^[17] The Pd/ZnO NW arrays after deposition were thermally annealed at 250 °C for 12 h. Applied voltage for deposition was determined from voltammetry cycles (not shown)^[17] and are presented in Table S1, Supporting Information. Figure S1, Supporting Information, shows growth curves for samples with different concentrations of PdCl₂ in the electrolyte at respective constant applied potential. Taking into account values of current density reported for pure ZnO NWs,^[18] by adding PdCl₂ in the electrolyte a dramatic increase of the deposition cathodic current density is obtained, which was also reported for ZnO:Ag NWs.^[17] Thus, we believe that Pd on the deposited structures serves as a good electrocatalyst for the electrochemical reactions. The experimental details on material characterization are presented in Supporting Information (Text S2). Computational details about DFT modeling and choice of the functionalized surface models are presented in Supporting Information (Text S3 and S4, respectively).

Morphological and Structural Properties of Pd/ZnO NW Arrays:

Figure 1 shows SEM images at different magnifications of Pd/ZnO NW arrays prepared from various concentrations of PdCl₂ in electrolyte: (a–c) 0.25 μM; (d–f) 0.50 μM; (g–i) 0.75 μM; (j–l) 1.00 μM; (m–o) 1.25 μM; (p–r) 1.50 μM. They are displayed from low magnification in the first column to high magnification in the third column. The details on pristine ZnO NW arrays and more informations about the influence of deposition parameters on the morphology are presented in our previous works.^[17–19]

The mechanism of ZnO NWs electrodeposition was already discussed in a previous work.^[18] The ZnO NWs have diameters in the range of $D = 100\text{--}200 \text{ nm}$ and lengths of $\approx 2.8\text{--}3.1 \mu\text{m}$.^[17] By adding PdCl₂ into the electrolyte, changes in aspect ratio and morphology of the NWs were observed (see Figure 1). The hexagonal shape of Pd modified ZnO NWs gradually disappears as the PdCl₂ concentration in the electrolyte increases toward the highest content. This tendency was also observed for Cd/ZnO NW arrays by ECD.^[18] The diameter of the NWs is decreased to about 100–150 nm when the PdCl₂ concentration is increased to 0.75 μM leading to more dense networks, while for further increase of the PdCl₂ concentration up to 1.5 μM, the diameter of the NWs considerably increases up to $\approx 500 \text{ nm}$ (see Figure 1p–r). The enhanced density of ZnO NWs was also observed in the case of Ag-doped ZnO NWs.^[17] It can be attributed to the electrocatalytic properties of PdCl₂ which favors the hydroxide ion generation at the beginning of the electrochemical growth.^[17] More representative SEM images of Pd modified ZnO NW arrays at low magnification to show overall view of networks and at much higher magnifications are presented in Figure S2, Supporting Information, for 0.25 μM, Figure S3, Supporting Information, for 0.50 μM, Figure S4, Supporting Information, for 0.75 μM, and Figure S5, Supporting Information, for 1.0 μM PdCl₂. Such rough surface and further increase in diameter (D) of Pd modified ZnO NW (for concentrations of PdCl₂ higher than 0.75 μM), that is ladder-like side surfaces and quite tapered tips of NWs (see Figure 1) can be attributed to the disturbance of the crystal growth in solution, where formation of native defects such as vacancies migrate to the surface and form pits, which was also observed for Cl- and Sb-doped ZnO NWs.^[20]

Figure 2a shows the effect of the Pd content in Pd/ZnO NW arrays on the crystallinity. The reflections marked with red asterisk (*) are assigned to tetragonal SnO₂ from FTO substrate according to JCPDS 01-088-0287 card.^[17] Others reflections are assigned to hexagonal ZnO crystalline phase according to JCPDS 00-036-1451 card. Reflections attributed to Pd, PdO or impurities were not observed, indicating that addition of PdCl₂ in the electrolyte does not change essentially the crystal structure of Pd/ZnO NWs.^[17] However, the reflections which are commonly observed in XRD patterns for Pd modified metal oxide nanostructures have the same values as ZnO main reflections and overlap it, thus it is difficult to distinguish Pd or PdO from ZnO by XRD.^[21] Higher intensity of reflection corresponding to (002) plane of the samples shows that the growth is along the c -axis normal to substrate as unambiguously demonstrated by TEM (see Figure S6, Supporting Information).^[17,22] The change in intensity of XRD reflection corresponding to (002) plane can be observed with increasing concentration of PdCl₂ in electrolyte, and this can be attributed to modifications in crystallinity of Pd/ZnO NWs.

No significant shift of reflections from XRD diffractograms by increasing PdCl₂ concentration in the electrolyte was observed. This suggests no detectable change of crystal lattice as a result of the similar ionic radii of Pd and Zn ($r(\text{Pd}^{2+}) = 0.078 \text{ nm}$ while $r(\text{Zn}^{2+}) = 0.074 \text{ nm}$).^[23] Thus, more likely Pd is not incorporated in the lattice of Pd-modified ZnO NWs during electrodeposition, although it can diffuse during the annealing process. To the best of our knowledge, reports with fair evidence of Pd doping in ZnO NWs are yet to be seen. This is probably due to low solubility of

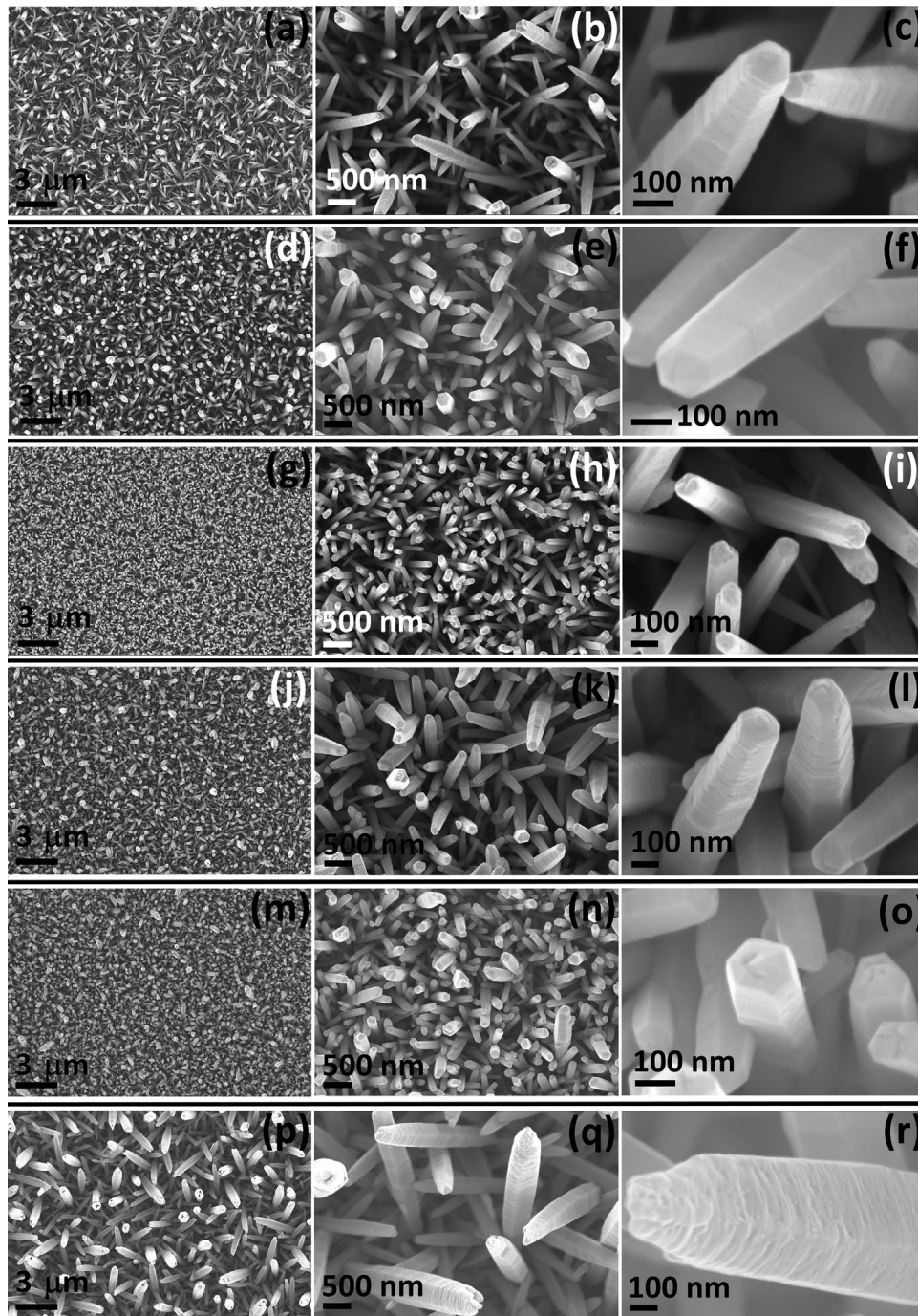


Figure 1. SEM images of Pd/ZnO NW arrays at different magnifications (from lower magnification in the first column to higher magnifications in the third column) and with different concentrations of PdCl₂ in the electrolyte (in μM): (a–c) 0.25; (d–f) 0.50; (g–i) 0.75; (j–l) 1; (m–o) 1.25; (p–r) 1.50.

Pd in ZnO.^[20] At the same time we see a bandgap shift (Figure 2b,c).

Pd modified ZnO NWs (with 0.75 μM Pd) were examined using TEM. Figure S6a, Supporting Information, shows the expected needle-like structure. The high resolution TEM (HRTEM) micrograph (the average background subtraction filter ABSF filtered) and the resulting fast Fourier transform (FFT) (see Figure S6b, Supporting Information) indicate that a needle-like

crystal grows along the *c*-direction. Figure S6c, Supporting Information, displays the selected area electron diffraction (SAED) pattern of a relatively larger and isolated ZnO needle (zone [2 -1 -1 0]). The measured *d*-values convincingly agree with values from literature for ZnO.^[24]

High angle annular dark field (HAADF)-STEM images reveal the presence of particles on the Pd modified ZnO NWs (0.75 μM of PdCl₂) with a size of about 20 nm. The density of

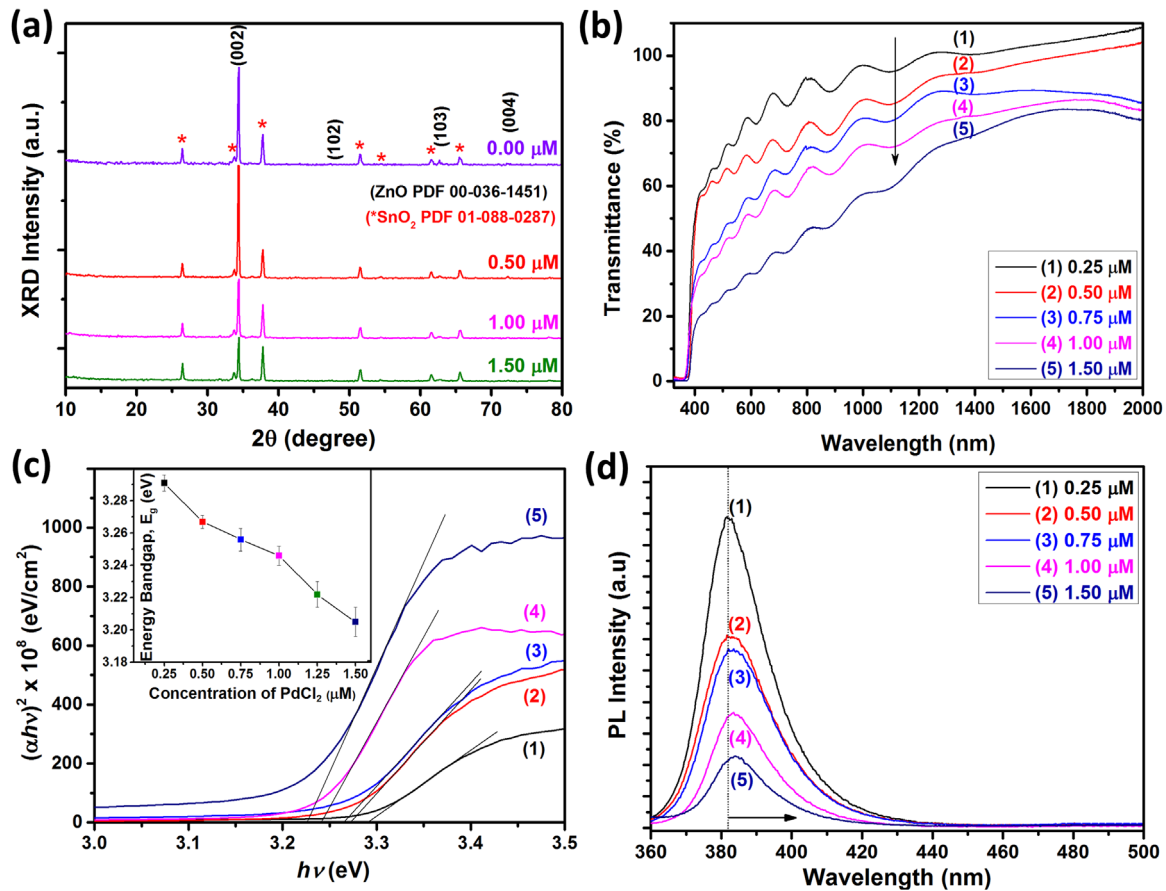


Figure 2. (a) XRD diffractograms; and (b) optical transmittance spectra of Pd/ZnO NW arrays. (c) Plot of $(\alpha h\nu)^2$ versus photon energy ($h\nu$). Inset: energy bandgap (E_g) versus concentration of PdCl₂ in electrolyte. (d) Room-temperature photoluminescence spectra of Pd/ZnO NW arrays.

these particles on the surface differs for different samples (see Figure 3a and e). Energy-dispersive X-ray spectroscopy (EDX) elemental maps show that these nanoparticles contain the Pd element (see Figure 3b–d). The oxidation state of Pd will be discussed based on X-ray photoelectron spectroscopy (XPS) data below, and we will show that these NPs are mainly formed by metallic Pd with low content of PdO.

The formation of Pd NPs on ZnO NWs surface can be explained based on electrodeposition from electrolyte solution with added PdCl₂ ($\text{Pd}^{2+}(\text{aq}) + 2\text{e}^- \rightarrow \text{Pd}(\text{s})$), which occurs with high current efficiency.^[5] However, the formation of films is stopped due to formation of Schottky barriers at Pd/ZnO NW interface, which blocks further deposition of Pd resulting in formation of NPs.^[25] This was also observed for other types of semiconductors.^[25]

Optical and Chemical Properties of Pd/ZnO NW Arrays: Figure 2b shows the room temperature UV-visible transmission spectra of Pd/ZnO NWs with different PdCl₂ concentrations in the electrolyte. A typical ZnO adsorption edge in the UV region can be observed for all samples. Similar to Ag/ZnO NWs and Cu/ZnO NWs, the decrease in the visible and near-infrared (NIR) range can be observed.^[17,25] For samples synthesized with 0.25 μM PdCl₂ in the electrolyte the transmittance is higher than 75% in the visible region and close to 90% in the near-infrared

region. By increasing the concentration of PdCl₂ in the electrolyte up to 1.25 μM the transmittance is decreased to 40% in the visible region and close to 60% in the NIR region. Figure 2c shows that the energy bandgap (E_g) shifts with higher PdCl₂ concentration in the electrolyte, thus making these materials quite interesting for optical applications.^[17,18,19,25] The inset of Figure 2c presents the estimated E_g versus concentration of PdCl₂ in the electrolyte. Because the incorporation of Pd into ZnO matrix was excluded, the slight decrease in bandgap energy can be explained by a change in the carrier concentration due to addition of Pd NPs.^[26] Also it was demonstrated that the addition of PdCl₂ in the reaction system can result in a reduction of oxygen vacancy concentration.^[26]

A considerable decrease in the intensity of PL emission at room temperature with an increase of the PdCl₂ concentration in the electrolyte can be observed in Figure 2d. However, for all samples no significant emission in the visible range due to defects is observed, demonstrating that Pd/ZnO NWs are of high quality, cf. supporting information in Figure S6a.^[17] Besides the decrease in the intensity of the near-band edge (NBE) emission peak, a slight shift toward higher wavelengths occurs with the increase of the Pd content.

Since TEM measurements showed the presence of Pd NPs in Pd modified ZnO NWs, the surface of the samples was further

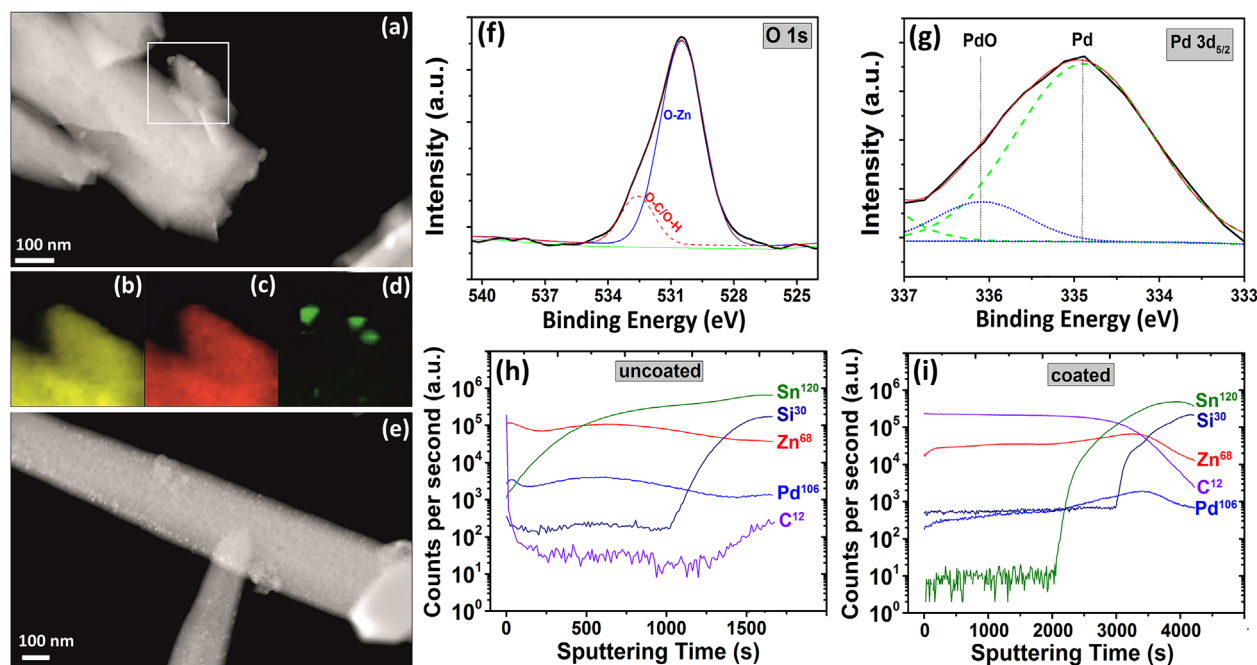


Figure 3. (a) HAADF-STEM image of ZnO crystals with few palladium nanoparticles. EDX elemental mapping showing: (b) Zn (L-line); (c) O (K-line); and (d) Pd (L-line) maps of the emphasized region in (a). (e) HAADF-STEM image of ZnO crystals with a higher amount of palladium nanoparticles from an additional sample. Higher resolution XPS spectrum of: (f) O-1s and (g) Pd-3d_{5/2} obtained from Pd modified ZnO NW arrays. SIMS measurements of: (h) uncoated and (i) photoresist-coated Pd modified ZnO NW arrays (0.75 μ M Pd) grown on FTO substrate.

analyzed by XPS in order to determine the oxidation state of Pd-NPs in more detail. The XPS sample was first partially spin-coated with S1813 photoresist at 300 RPM for 60 s. After spin-coating, the sample was annealed at 115 °C for 60 s. In XPS survey spectra of uncoated sample grown by adding 0.75 μ M of PdCl₂ in the electrolyte without pre-cleaning procedure (Figure S7, Supporting Information), Zn, O, Pd, C elements were detected. A relatively high concentration of adventitious carbon (\approx 35%) was detected.^[22] Inset in Figure S6, Supporting Information shows the XPS spectra of the Zn-2p_{2/3} core level regions of ZnO:Pd NWs at 1022.2 eV. The asymmetric O-1s peak from Figure 3f was deconvoluted by two subspectral components corresponding to ZnO (530.3 eV) and defective ZnO_x and/or Zn-OH species (532.6 eV).^[22] The line intensity of Pd-3d_{5/2} core level emission peaks of the Pd modified ZnO NWs is presented in Figure 3g. A detailed peak analysis suggests a superposition of two peaks located at 334.9 and 336.1 eV which are attributed to Pd and PdO, respectively (see Figure 3g).^[27] The oxide formation of Pd can be the result of the interaction with water vapor in ambient air or interaction with oxygen from growth solution during the ECD deposition.^[17,28]

The chemical composition of Pd modified ZnO NW arrays (0.75 μ M of PdCl₂) grown on FTO substrate was further investigated using SIMS measurements. Figure 3h shows the results of uncoated arrays, that is Zn, Sn, Pd, Si, and C signals versus sputtering time. Sn signal originated from FTO substrate appears very early in the measurement and do not follow the rate of Zn signal, which means that the ZnO NW arrays are not very dense, so the ion beam can sputter the bottom substrate (FTO).^[6,16] At sputtering time of 1000 s, the Si signal starts to increase, which means the FTO film on the glass, has been

removed due to sputtering, so the Si signal from the glass substrate appears. The C signal is originating from surface contamination of top ZnO NW arrays, which is confirmed by a very sharp decrease at the beginning of sputtering.^[16] In the case of photoresist coated Pd/ZnO NW arrays (see Figure 3i) the Sn signal does not appear until 2000 s and then rises very sharply. It means that the photoresist prevents the ion beam from penetrating into the aligned ZnO NWs. The C signal with high intensity originates from photoresist, and it is more or less uniform until one penetrates into the glass. As in the case of uncoated samples, the Pd signal tracks very close Zn signal. The experiment suggests that the Pd content is about 0.15–0.20 at.% in this sample.^[6,16] Also, the Si signal in the case of photoresist coated samples starts around 3000 seconds. This occurs when the photoresist and FTO substrate both are sputtered away and the glass signal (Si) starts to appear.

Modulation of Structural and Electronic Properties Upon Doping – Theoretical Insights: From the above discussions, the Pd-doping in bulk of ZnO nanowires was not demonstrated. However, traces of surface doping and functionalization of Pd/ZnO NWs, can be clearly seen. Consequently, to get a better overview of possible Pd/ZnO structures, we present data obtained on models of Pd-doped bulk ZnO wurtzite and adsorption of Pd clusters of different sizes on the undoped and doped ZnO (1 0 -1 0) surface, as an example of surface functionalization. As already done for Cd,^[16,18] Cu,^[29] and Ag,^[8,17] calculations have been performed on: (i) pure ZnO, (ii) Pd-doped ZnO, at three different amounts (0.78, 1.85, and 6.25 at.%) and Pd; only at the 1.85 at.% amount, as an example of the effect of the Pd amount on structures and electronic properties. Obtained data are collected in Table S2, Supporting

Information, and unit cells are shown in Figure S8, Supporting Information.

From the computed shortest metal to O distances (d_1 to d_6 in Table S2, Supporting Information), when substituting, it is clear that the coordination of the metal goes from tetrahedral in pure ZnO with significantly different values for d_1 and d_5 (see Figure S8e, Supporting Information), to an almost regular triangular bipyramid when considering substitution at 6.25 at%, with similar d_1 and d_5 values. Consequently, an increase of in the a and b lattice parameters and a decrease of in c are obtained in the doped material when compared with pure ZnO. Upon insertion however, a distorted octahedron can be evidenced, with three long (≈ 2.7 Å) and three shorter distances (≈ 2.3 Å). In that case, all three lattice vectors are slightly increased, due to the larger Pd radius compared to that of Zn, evidencing that Pd incorporation in the experimental samples is probably mostly due to both substitution and adsorption. These geometrical distortions can all be related to a Jahn-Teller effect. From the data of Figure S9 and Table S2, Supporting Information, it is clear that the ZnO band gap decreases upon Pd contents, by at least 1.2 eV in agreement with experimental data (therefore the modeling shows the Pd doping). For substitution, Pd contributes mainly at the top of the valence band (VB) and the bottom of the conduction band (CB), establishing bands with low dispersion and an almost atomic-like character. However, for concentrations of 6.25 at.% a small overlap with O_{2p} states can be evidenced, indicating a larger hybridization of Pd_{4d} and O_{2p} orbitals. When substituting, a shallow level can be found in the ZnO band gap indicating p -type ZnO formation, as already obtained in the case of Ag doping.^[17] Similar conclusions can be drawn for insertion, but the lack of shallow level at the bottom of the CB indicates that no p -type ZnO is obtained.

Adsorption of small Pd_n clusters (n ranging from 1 to 9) on a ZnO (1 0 -1 0) slab^[17,30] has also been considered (see Figure 4).

Comments on the functionalized surface models can be found in the Supporting Information (Text S3).

From the data collected in Table S3, Supporting Information, it is clear that the larger the Pd_n cluster is, the larger is the adsorption energy and the smaller the electronic band gap. Larger clusters show a larger spread over the ZnO surface, leading to larger adsorption energies due to the increasing number of Pd-O and Pd-Zn bonds between the adsorbate and the substrate. For Pd_1 and Pd_2 clusters, Pd preferentially adsorbs in bridge sites that are in-between Pd and O atoms. For larger clusters, hollow sites are populated, leading to an hexagonal close packed (*hcp*) motif on top of the ZnO substrate. Although the obtained band gap values for all adsorbed systems differ significantly from those reported experimentally in Figure 2c, it should be noted that: (i) the trend of decreasing E_g upon increase of the $PdCl_2$ concentration in the electrolyte is qualitatively reproduced; (ii) the computed band gap of the pure ZnO (1 0 -1 0) surface of 3.89 eV nicely reproduces that of the pure ZnO NW obtained by experiments,^[18] thus validating our model. Increasing concentration of Pd leading to atomic substitution within the ZnO slab (system Pd_9/ZnO) has also been considered, but only a slight variation of computed band gaps could be evidenced (<10%).

From Figure S10, Supporting Information, as already found for the bulk system, weakly-interacting Pd_{4d} levels contribute mainly to the band gap decrease observed for the functionalized surface. However, shallow levels can only be evidenced at the bottom of the CB for clusters larger than Pd_3 , outlining the role of the NP size in determining the electronic structure of these surfaces, and hence the possibility of strongly influencing their reactivity, by tuning the Pd cluster sizes.

High Performance Nanosensor Based on Individual Pd/ZnO NWs: Based on single Pd/ZnO NW with different Pd contents, NWs with diameter (D) of approximately 160 nm and length about

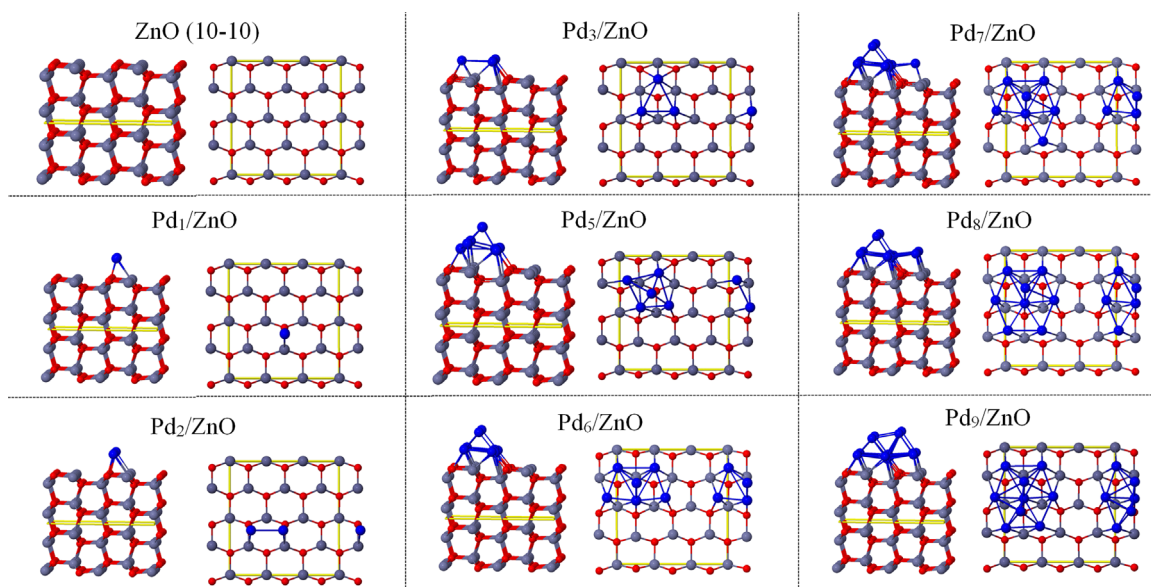


Figure 4. Side and top views of the unit cells of the pure ZnO (1 0 -1 0) surface with 8 layers, and of Pd_n/ZnO (1 0 -1 0), with n ranging from 1 to 9. Red, grey and blue balls represent O, Zn, and Pd atoms, respectively. Unit cell as solid yellow line is shown.

1.4 μm were fabricated (i.e., practically the same aspect ratio), and several devices were tested at 100 ppm H_2 at room temperature and relative humidity (RH) of 30% RH. It is important to maintain the same aspect ratio because the diameter of individual nanostructures has a larger influence on gas sensing properties.^[6,16] Figure 1 demonstrates that the PdCl_2 content in electrolyte solution influences the aspect ratio of Pd/ZnO NWs. Thus, if it was the case of sensors based on arrays of Pd/ZnO NWs, the aspect ratio should have been taken into account.

Results on hydrogen response of single ZnO NW nanosensors (diameter of ≈ 160 nm) versus PdCl_2 concentration and gas response of nanosensors to different types of reducing gases are presented in Figure 5a,b. Inset of Figure 5b shows a typical SEM image of nanosensors based on a single Pd/ZnO NW with $D \approx 160$ nm and grown in the electrolyte with 0.75 μM of PdCl_2 . In Figure S11, Supporting Information, a typical current-voltage characteristic at room temperature of the nanosensor device (Pd/ZnO NW grown in the electrolyte with 0.75 μM of PdCl_2) is presented. Formation of double Schottky contacts is due to the Pt contacts, that has higher work function than that of Pt contact when compared to ZnO.^[31] All fabricated devices in this study showed the same behavior of current-voltage characteristics (not shown).

As can be observed from Figure 5a, the hydrogen response ($I_{\text{H}_2}/I_{\text{air}}$) is promoted and strongly enhanced from ≈ 1.5 to about 13100 (about four orders of magnitude increase!) by increasing PdCl_2 concentration in the electrolyte from 0.25 to 0.75 μM . A further increase in PdCl_2 concentration to 1.5 μM resulted in a decrease down to ≈ 9.2 . Thus, the optimal PdCl_2 concentration in the electrolyte for growth of Pd/ZnO NWs is determined to be 0.75 μM (see Figure 5a). The response value is much higher than for single pristine ZnO NW, Ag/ZnO,^[8,17] and Cd/ZnO,^[16] NW or other single and networked semiconducting nanostructures (see Table S4, Supporting Information). Next the selectivity of a

nanosensor based on Pd/ZnO NW (0.75 μM of PdCl_2) was investigated by exposure to 100 ppm of CO_2 , CH_4 , ethanol and acetone vapor (see Figure 5b). To evaluate the selectivity of H_2 gas nanosensor the ratio of the gas responses were used, i.e. the ratio of hydrogen gas response (S_{H_2}) and of gas response to other gases. The results of $S_{\text{H}_2}/S_{\text{CO}} \approx 2848$, $S_{\text{H}_2}/S_{\text{CH}_4} \approx 2339$, $S_{\text{H}_2}/S_{\text{EtOH}} \approx 1065$, and $S_{\text{H}_2}/S_{\text{Acetone}} \approx 2079$ show excellent selectivity to H_2 gas.

The dynamic response of the nanosensors is presented in Figure 5c for a device based on a Pd/ZnO NW grown in the electrolyte solution with 0.75 μM of PdCl_2 , and in Figure S12, Supporting Information, for devices with different concentrations of PdCl_2 , respectively. Up to 0.75 μM the nanosensor response is rapidly approaching the saturation value (see Figure 5c and Figure S12a,b, Supporting Information), while the response of devices based on a Pd/ZnO NW grown in the electrolyte solution with concentration of PdCl_2 higher than 0.75 μM is still increasing even after exposure to H_2 gas for 30 s (see Figure S12c,d, Supporting Information). The response time (t_r) and recovery time (t_d) were calculated and generalized in Figure S13a and Table S5, Supporting Information, which clearly show that t_r and t_d values are decreasing up to 0.75 μM of PdCl_2 in the electrolyte and that these values are increasing with a further increase of the PdCl_2 concentration. This can be explained based on an enhanced rate of catalytic activity of Pd/ZnO NW by increasing Pd content.^[10,12,14] However at higher content of Pd in a Pd/ZnO NW, the catalytic activity is much pronounced which gives higher concentration of catalytic centers and lowers the saturation rate of the response and recovery process.^[10,12,14]

The lowest detection limit (LDL) for H_2 detection of a nanosensor based on Pd/ZnO NW (0.75 μM of PdCl_2) was approximated by linear fitting from Figure S13b, Supporting

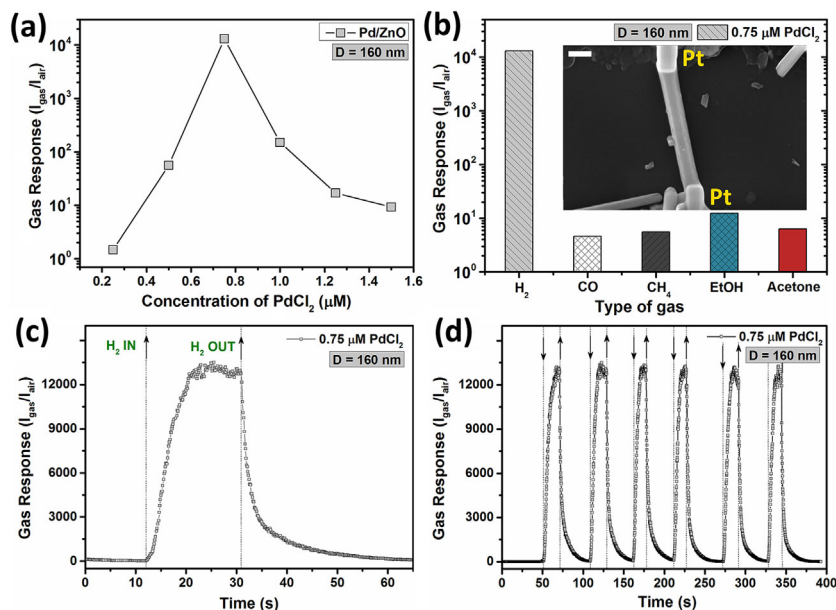


Figure 5. (a) Hydrogen response of a single ZnO NW nanosensor with a diameter of ≈ 160 nm versus concentration of PdCl_2 in electrolyte. (b) Gas response of nanosensors to different types of reducing gases. The inset is a SEM image of the nanosensor (the scale bar is 200 nm). (c,d) Dynamic hydrogen gas response to single and multiple pulses are presented, respectively.

Information, with response criteria $I_{\text{gas}}/I_{\text{air}} > 1.2$ and showed sub-ppm value beyond 0.015 ppm. This value is lower than that for previously reported sensors on Fe-doped ZnO^[22] or Zn-doped CuO and Cu₂O nanostructured films,^[6,32] Pd coated Si NWs,^[33] single TeO₂ NW.^[34] This finding demonstrates that our optimized Pd/ZnO NW sensor possesses one of the lowest detection limits among oxide-based hydrogen sensors.^[10,22,33,34] Also, the detection limit is much lower than that reported for most of the commercial hydrogen gas sensors for industrial, environmental, and military monitoring.^[33] This outstanding performance could be based on the very high surface-to-volume ratio of the NWs and the high catalytic activity of Pd.^[7,13,15,33] In conclusion, the optimal content of PdCl₂ in the electrolyte for growth of Pd/ZnO NW with ultra-sensitive and highly selective detection of H₂ gas is 0.75 μM. Figure 5d shows the repeatability and stability of the fabricated nanosensor based on a Pd/ZnO NW (0.75 μM of PdCl₂ and $D \approx 160$ nm) with a deviation in the gas response lower than 5%. The gas sensing mechanism is discussed in Supporting Information (Text S1) and was also discussed in detail in our previous work.^[35] The high selectivity to H₂ gas of Pd-modified ZnO NWs can be explained based on low hydrogen-binding energy of Pd, as well as its low energy barriers for hydrogen dissociation with further formation of PdH_x with different properties.^[36]

Another important factor is the formation of the Schottky contacts (at the Pt/ZnO NW interface) which is known to be highly selective to hydrogen gas.^[37] After catalytic chemical adsorption of H₂ gas molecules on Pt with further diffusion through Pt layer, a dipole layer is formed at the Pt/ZnO interface.^[37] This reduces the Schottky barrier height and induces a considerable change in the device current.^[37] More details on this mechanism are presented in Refs.^[37]

In summary, Pd/ZnO NW arrays were synthesized onto FTO substrate by electrodeposition at 90 °C using a method for surface doping and functionalization in a one-step process. The advantage of this procedure is to combine growth, surface doping, and functionalization of Pd/ZnO NWs by using ECD, and to reduce essentially the number of technological steps for nanomaterial and final nanodevices fabrication. Different techniques of material characterization, such as XRD, Raman, XPS, and TEM have demonstrated the high crystallinity of the Pd/ZnO NWs synthesized over a wide range of PdCl₂ concentrations in the electrolyte (0.25 to 1.50 μM). Single NWs of Pd/ZnO with different concentrations of Pd were integrated into nanosensors using a FIB/SEM system. The gas sensing properties were investigated in detail. The influence of the PdCl₂ concentration was studied and revealed a high gas response for Pd/ZnO NW ($D \approx 160$ nm) grown in the electrolyte with 0.75 μM of PdCl₂. An ultra-high response or a giant response of $I_{\text{gas}}/I_{\text{air}} \approx 13100$ were obtained to 100 ppm of H₂ gas at room temperature and 30% RH. Excellent selectivity was demonstrated by testing with other types of reducing gases, and demonstrated negligible response compared to those of H₂ gas. The excellent H₂ gas sensing properties of the Pd/ZnO NW have been explained based on improved catalytic properties due to Pd NPs surface functionalization. DFT calculations performed on Pd-doped ZnO bulk and functionalized surface models allowed to support and further validate the model proposed based on the experimental findings.

Supporting Information

Supporting Information is available from the Wiley Online Library or from the authors.

Acknowledgements

Dr. Lupan acknowledges the Alexander von Humboldt Foundation for the research fellowship for experienced researchers 3-3MOL/1148833 STP at the Institute for Materials Science, University of Kiel, Germany. This research was funded partially by the German Research Foundation (DFG) under the scheme SFB 1261 and FOR2093. This work was partially supported by the STCU within the Grant 6229.

Conflict of Interest

The authors declare no conflict of interest.

Keywords

gas sensors, hydrogen, nanowires, palladium, ZnO

Received: September 15, 2017

Revised: November 4, 2017

Published online: November 20, 2017

- [1] (a) T. K. Sau, A. L. Rogach, *Adv. Mater.* **2010**, *22*, 1781; (b) T. K. Sau, A. L. Rogach, F. Jäckel, T. A. Klar, J. Feldmann, *Adv. Mater.* **2010**, *22*, 1805; (c) M. V. Seregina, L. M. Bronstein, O. A. Platonova, D. M. Chernyshov, P. M. Valetsky, J. Hartmann, E. Wenz, M. Antonietti, *Chem. Mater.* **1997**, *9*, 923; (d) W. Shenton, S. A. Davis, S. Mann, *Adv. Mater.* **1999**, *11*, 449.
- [2] F. Favier, E. C. Walter, M. P. Zach, T. Benter, R. M. Penner, *Science* **2001**, *293*, 2227.
- [3] A. Kolmakov, D. O. Klenov, Y. Lilach, S. Stemmer, M. Moskovits, *Nano Lett.* **2005**, *5*, 667.
- [4] S. Sakthivel, M. V. Shankar, M. Palanichamy, B. Arabindoo, D. W. Bahnemann, V. Murugesan, *Water Res.* **2004**, *38*, 3001.
- [5] (a) N. Yamazoe, *Sens. Actuators B* **1991**, *5*, 7; (b) F. Yang, D. K. Taggart, R. M. Penner, *Nano Lett.* **2009**, *9*, 2177.
- [6] O. Lupan, V. Cretu, V. Postica, O. Polonskyi, N. Ababii, F. Schütt, V. Kaidas, F. Faupel, R. Adelung, *Sens. Actuators B* **2016**, *230*, 832.
- [7] M. Hübner, N. Bârsan, U. Weimar, *Sens. Actuators B* **2012**, *171-172*, 172.
- [8] C. Liu, Q. Kuang, Z. Xie, L. Zheng, *CrystEngComm* **2015**, *17*, 6308.
- [9] X. Liu, N. Chen, B. Han, X. Xiao, G. Chen, I. Djerdj, Y. Wang, *Nanoscale* **2015**, *7*, 14872.
- [10] E. Şennik, O. Alev, Z. Z. Öztürk, *Sens. Actuators B* **2016**, *229*, 692.
- [11] M. G. Chung, D.-H. Kim, D. K. Seo, T. Kim, H. U. Im, H. M. Lee, J.-B. Yoo, S.-H. Hong, T. J. Kang, Y. H. Kim, *Sens. Actuators B* **2012**, *169*, 387.
- [12] N. Y. Chan, M. Zhao, J. Huang, K. Au, M. H. Wong, H. M. Yao, W. Lu, Y. Chen, C. W. Ong, H. L. W. Chan, J. Dai, *Adv. Mater.* **2014**, *26*, 5962.
- [13] Y. C. Lee, H. Huang, O. K. Tan, M. S. Tse, *Sens. Actuators B* **2008**, *132*, 239.
- [14] C.-M. Chang, M.-H. Hon, I.-C. Leu, *ACS Appl. Mater. Interfaces* **2013**, *5*, 135.
- [15] Y. Hu, J. Zhou, P.-H. Yeh, Z. Li, T.-Y. Wei, Z. L. Wang, *Adv. Mater.* **2010**, *22*, 3327.

- [16] (a) O. Lupan, L. Chow, T. Pauporté, L. K. Ono, B. Roldan, Cuenya, G. Chai, *Sens. Actuators B* **2012**, 173, 772; (b) O. Lupan, V. Postica, J. Gröttrup, A. K. Mishra, N. H. de Leeuw, R. Adelung, *Sens. Actuators B* **2017**, 245, 448; (c) F. Schütt, V. Postica, R. Adelung, O. Lupan, *ACS Appl. Mater. Interfaces* **2017**, 9, 23107.
- [17] T. Pauporté, O. Lupan, J. Zhang, T. Tugsuz, I. Ciofini, F. Labat, B. Viana, *ACS Appl. Mater. Interfaces* **2015**, 7, 11871.
- [18] (a) O. Lupan, T. Pauporté, T. Le Bahers, I. Ciofini, B. Viana, *J. Phys. Chem. C* **2011**, 115, 14548; (b) T. Pauporté, D. Lincot, *J. Electrochem. Soc.* **2001**, 148, C310; (c) A. Goux, T. Pauporté, J. Chivot, D. Lincot, *Electrochim. Acta* **2005**, 50, 2239; (d) T. Pauporté, G. Bataille, L. Joulaud, F. J. Vermersch, *J. Phys. Chem. C* **2010**, 114, 194.
- [19] (a) O. Lupan, B. Viana, T. Pauporté, M. Dhaouadi, F. Pellé, L. Devys, T. Gacoin, *J. Phys. Chem. C* **2013**, 117, 26768; (b) O. Lupan, T. Pauporté, V. V. Ursaki, I. M. Tiginyanu, *Optic. Mater.* **2011**, 33, 914; (c) O. Lupan, T. Pauporté, I. M. Tiginyanu, V. V. Ursaki, H. Heinrich, L. Chow, *Mater. Sci. Eng. B* **2011**, 176, 1277; (d) O. Lupan, T. Pauporté, B. Viana, P. Aschehoug, M. Ahmadi, B. R. Cuenya, Y. Rudzevich, Y. Lin, L. Chow, *Appl. Surf. Sci.* **2013**, 282, 782.
- [20] (a) F. Wang, J.-H. Seo, Z. Li, A. V. Kvit, Z. Ma, X. Wang, *ACS Appl. Mater. Interfaces* **2014**, 6, 1288; (b) J. K. Liang, H. L. Su, C. L. Kuo, S. P. Kao, J. W. Cui, Y. C. Wu, J. C. A. Huang, *Electrochim. Acta* **2014**, 125, 124; (c) O. Lupan, T. Pauporté, L. Chow, B. Viana, F. Pellé, B. Roldan Cuenya, L. K. Ono, H. Heinrich, *Appl. Surf. Sci.* **2010**, 256, 1895.
- [21] Q. Li, Y. W. Li, P. Wu, R. Xie, J. K. Shang, *Adv. Mater.* **2008**, 20, 3717; Q. Li, R. Xie, E. A. Mintz, J. K. Shang, *J. Am. Ceram. Soc.* **2007**, 90, 3863.
- [22] I. Hölken, G. Neubüser, V. Postica, L. Bumke, O. Lupan, M. Baum, Y. K. Mishra, L. Kienle, R. Adelung, *ACS Appl. Mater. Interfaces* **2016**, 8, 20491.
- [23] R. Shannon, *Acta Crystallogr. A* **1976**, 32, 751.
- [24] H. Sowa, H. Ahsbahs, *J. Appl. Crystallogr.* **2006**, 39, 169.
- [25] (a) H. Hasegawa, T. Sato, *Electrochim. Acta* **2005**, 50, 3015; (b) O. Lupan, T. Pauporté, B. Viana, P. Aschehoug, *Electrochim. Acta* **2011**, 56, 10543.
- [26] Y. Chang, J. Xu, Y. Zhang, S. Ma, L. Xin, L. Zhu, C. Xu, *J. Phys. Chem. C* **2009**, 113, 18761.
- [27] G. Ketteler, D. F. Ogletree, H. Bluhm, H. Liu, E. L. D. Hebenstreit, M. Salmeron, *J. Am. Chem. Soc.* **2005**, 127, 18269.
- [28] M. Moroseac, T. Skála, K. Veltruská, V. Matolín, I. Matolínová, *Surf. Sci.* **2004**, 566-568, Part 2, 1118.
- [29] O. Lupan, T. Pauporté, T. Le Bahers, B. Viana, I. Ciofini, *Adv. Funct. Mater.* **2011**, 21, 3564.
- [30] F. Labat, I. Ciofini, C. Adamo, *J. Chem. Phys.* **2009**, 131, 044708.
- [31] Z. L. Wang, J. Song, *Science* **2006**, 312, 242.
- [32] V. Cretu, V. Postica, A. K. Mishra, M. Hoppe, I. Tiginyanu, Y. K. Mishra, L. Chow, N. H. de Leeuw, R. Adelung, O. Lupan, *J. Mater. Chem. A* **2016**, 4, 6527.
- [33] J.-S. Noh, H. Kim, B. S. Kim, E. Lee, H. H. Cho, W. Lee, *J. Mater. Chem.* **2011**, 21, 15935.
- [34] C. Yan, B. Huy Le, D. J. Kang, *J. Mater. Chem. A* **2014**, 2, 5394.
- [35] O. Lupan, V. Postica, F. Labat, I. Ciofini, T. Pauporté, R. Adelung, *Sens. Actuators B* **2018**, 254, 1259.
- [36] (a) T.-R. Rashid, D.-T. Phan, G.-S. Chung, *Sens. Actuators B* **2013**, 185, 777; (b) X. Q. Zeng, M. L. Latimer, Z. L. Xiao, S. Panuganti, U. Welp, W. K. Kwok, T. Xu, *Nano Lett.* **2011**, 11, 262; (c) V. Postica, F. Schütt, R. Adelung, O. Lupan, *Adv. Mater. Interfaces* **2017**, 4, 1700507.
- [37] (a) V. Postica, J. Gröttrup, R. Adelung, O. Lupan, A. K. Mishra, N. H. de Leeuw, N. Ababii, J. F. C. Carreira, J. Rodrigues, N. B. Sedrine, M. R. Correia, T. Monteiro, V. Sontea, Y. K. Mishra, *Adv. Funct. Mater.* **2017**, 27, 1604676; (b) S. N. Das, J. P. Kar, J.-H. Choi, T. I. Lee, K.-J. Moon, J.-M. Myoung, *J. Phys. Chem. C* **2010**, 114, 1689; (c) O. Lupan, V. Postica, N. Wolff, O. Polonskyi, V. Duppel, V. Kaidas, E. Lazari, N. Ababii, F. Faupel, L. Kienle, R. Adelung, *Small* **2017**, 13, 1602868.